# Modeling solid–solid phase transitions in PETN using density functional theory

Cite as: AIP Conference Proceedings **1979**, 040004 (2018); https://doi.org/10.1063/1.5044782
Published Online: 03 July 2018

Nam Q. Le, and Igor V. Schweigert



# Modeling Solid–Solid Phase Transitions in PETN Using Density Functional Theory

Nam Q. Le[1, 2, a)] and Igor V. Schweigert[1, b)]

[1]*U.S. Naval Research Laboratory, Code 6189, 4555 Overlook Ave. SW, Washington, D.C. 20375, United States*
[2]*NRC Postdoctoral Associate*

[a)] Corresponding authors: nam.le.ctr@nrl.navy.mil
[b)] igor.schweigert@nrl.navy.mil

**Abstract.** We present density functional theory (DFT) calculations of a stable orthorhombic phase of hydrostatically compressed pen-taerythritol tetranitrate (PETN). In these calculations, an orthorhombic ($a \neq b \neq c$) structure optimized at a very high pressure was used to initialize crystal structure optimizations at progressively lower pressures until the optimization spontaneously reverted to a tetragonal phase ($a = b \neq c$). The orthorhombic crystal structures exhibit $P2_12_12$ symmetry and a lowering of molecular symmetry from $S_4$ to $C_2$, which matches the orthorhombic PETN III phase debated in the literature. These findings are consistent across several DFT methods; however, the predicted transition pressures range from 16 to 23 GPa depending on the type of the functional and the size of the periodic supercell.

## INTRODUCTION

Pentaerythritol tetranitrate (PETN), a crystalline nitrate ester, is used extensively in detonating fuses and exploding bridgewire detonators. Tailoring its behavior under shock compression and transition to detonation is important for reliability and safety of these devices [1, 2]. PETN is known to exhibit an unusual anisotropic response to shock compression: crystals shocked normal to the (110) and (001) planes detonate at shock pressure between 4 and 8.6 GPa, but remain inert up to 19 GPa when shocked normal to the (100) or (101) planes. Steric hindrance to shear [2], anisotropic heating [3], and polarizations of the crystal lattice [4] have been proposed as possible mechanisms of the anisotropic sensitivity. A shock-induced transition from its ambient tetragonal phase [5] to a lower-symmetry phase has also been suggested to contribute to the anisotropic response. The existence of a stable orthorhombic phase of PETN at GPa pressures has been debated in the literature and is the subject of this study.

Gruzdkov et al. [4] were first to observe peak splittings in the Raman spectra of PETN powder above 5 GPa using glycerol as a pressure medium. They attributed the changes to the lowering of molecular symmetry from $S_4$ to $C_2$ and a transition from a tetragonal unit cell (space group $P\bar{4}2_1c$) to an orthorhombic unit cell ($P2_12_12$). This symmetry assignment was corroborated by comparing calculated Raman spectra of various conformers of gas-phase PETN, wherein lower-symmetry conformers exhibited peak splittings and shifts in qualitative agreement with the measured changes in compressed PETN.

Lipinska-Kalita, Pravica, and co-workers [6–8] observed the appearance of new lines in the powder X-ray diffrac-tion (XRD) of neat PETN above 8 GPa and in PETN mixed with KBr above 6 GPa. They attributed the changes to an incomplete phase transition with the presence of an orthorhombic phase. However, they did not observe peak splittings in the Raman spectra up to 10 GPa in PETN powder when using $N_2$ as a pressure medium. They concluded that the phase transition was induced by non-hydrostatic stresses present in neat PETN but not in the $N_2$ pressure medium.

Ciezak and Jenkins [9] observed peak splittings between 6 and 9 GPa in Raman spectra of PETN powder using Ne as a pressure medium. They also observed changes in Raman spectra of single-crystal PETN using $N_2$, Ne, and He as pressure media, but found that the threshold pressures varied significantly with the pressure medium [9]. They concluded that the appearance of the new phase is correlated with the onset of non-hydrostatic response of the pressure medium. They also observed an onset of plastic deformation at pressures above 14 GPa.

*Shock Compression of Condensed Matter - 2017*
AIP Conf. Proc. 1979, 040004-1–040004-6; https://doi.org/10.1063/1.5044782
Published by AIP Publishing. 978-0-7354-1693-2/$30.00

Dreger and Gupta [10] reported Raman spectra and optical images of single-crystal PETN using glycerol and Ar as the pressure media and confirmed the onset of a new phase at about 5 GPa for glycerol and 9 GPa for Ar [10]. They also reported evidence of another orthorhombic phase in the temperature range 389–399 K and proposed that the new high-temperature/high-pressure phase corresponds to further lowering of the molecular symmetry from $C_2$ to $C_1$.

Previous DFT calculations of crystalline PETN mostly focused on the tetragonal phase at ambient pressure [11, 12] and under hydrostatic compression [13–19]. To our knowledge, no DFT calculations have described a stable orthorhombic phase of PETN. Gan et al. [14] modeled hydrostatic compression of PETN I up to 25 GPa and reported that breaking the tetragonal symmetry did not result in a lower-energy orthorhombic structure. Ciezak et al. [20] used a crystal structure prediction method and a classical interatomic potential to generate possible orthorhombic structures, but found that subsequent DFT optimizations reverted to tetragonal structures. Tschauner et al. [8] used DFT to relax atomic coordinates while keeping the lattice constants fixed to their measured values, but found that the resulting orthorhombic structure exhibited nonhydrostatic stresses on the scale of 1 GPa. They also found that the tetragonal structure optimized with the same cell volume had lower enthalpy [8].

In this work, we performed DFT-based crystal structure calculations wherein both atomic coordinates and lattice constants were simultaneously optimized to obtain stationary electronic energies under prescribed external pressures from 0 to 36 GPa. To circumvent the apparent metastability of the tetragonal structure at higher pressures, we used an orthorhombic structure optimized at 30 GPa to initialize optimizations at progressively lower pressures. As a result, we were able to converge tetragonal structures at all pressures and orthorhombic structures above a certain pressure. We also estimated the enthalpies of the structures (not including zero-point energy or thermal corrections) and found that, when available, the converged orthorhombic structures have lower enthalpies than the tetragonal ones. The crystal structure and molecular symmetry of the predicted orthorhombic phase were analyzed and found to match the reported symmetry of PETN III. These findings were consistent among multiple DFT methods, using generalized-gradient and hybrid functionals with and without dispersion corrections. However, the transition pressure is surprisingly sensitive to the DFT method; among the methods tested here, predictions of the transition pressure range from about 16 GPa to 23 GPa.

## COMPUTATIONAL METHODS

DFT calculations were performed using the mixed Gaussian and plane wave method (GPW) as implemented in CP2K [21]. The generalized gradient functional of Perdew, Burke, and Ernzerhof (PBE) [22] and hybrid functional of Heyd, Scuseria, and Ernzerhof (HSE) [23] were combined with double- and triple-$\zeta$ Gaussian basis sets augmented with polarization functions (DZVP and TZVP). The Geodecker–Teter–Hutter (GTH) pseudopotentials [24, 25] and 600 Rydberg kinetic energy cutoff in the plane-wave-based Poisson solver were used in all calculations. Calculations with the PBE functional also used Grimme's semiempirical D2 [26] and D3 [27] corrections for long-range dispersion interactions with a cutoff radius of 12 Å in addition to uncorrected PBE calculations. Most calculations used a $1\times1\times2$ supercell containing 4 PETN molecules. PBE calculations were also repeated with a $2\times2\times2$ supercell containing 16 PETN molecules to test for finite size effects. Only the $\Gamma$ point of the Brillouin zone was sampled in all calculations.

Atomic coordinates and lattice constants were optimized simultaneously under prescribed external hydrostatic pressures from 0 to 36 GPa. The Broyden–Fletcher–Goldfarb–Shanno algorithm was used to minimize root-mean-square force within $3\times10^{-4}$ Ha/bohr and root-mean-square displacement between iterations within $1.5\times10^{-3}$ bohr. For each reported structure, the pressure was converged within 20 bar of the target pressure. The unit cell vectors were constrained to remain orthogonal in all calculations. Symmetry analysis of converged structures was performed using the FINDSYM program of Stokes et al. [28].

In order to estimate the relative thermodynamic stability of each structure, we also calculated the enthalpy as $H = E_{\text{elec}} + PV$, where $E_{\text{elec}}$ is the total electronic internal energy, $P$ is the pressure, and $V$ is the molar volume. We note that this does not include the zero-point energy (ZPE) in lattice vibrations. Preliminary calculations indicate that obtaining ZPE corrections will require vibrational frequencies based on geometry optimizations using stricter convergence criteria, which we are currently performing.

## RESULTS AND DISCUSSION

Optimizations at the PBE-D3/DZVP level with the $1\times1\times2$ supercell initiated with the tetragonal PETN I crystal structure from Zhurova et. al. [11] invariably preserved the tetragonal symmetry of the initial structure, resulting in

**TABLE 1.** Comparison between the PETN I lattice parameters obtained at the PBE-D3/DZVP level and prior theoretical and experimental values.

| | **PBE-D3** 0 K | **PBE [14]** 0 K | **PBE-D2[19]** 0 K | **XRD [11]** 100 K | **XRD [29]** 300 K |
|---|---|---|---|---|---|
| $a = b$ (Å) | 9.436 | 9.425 | 9.276 | 9.276 | 9.383 |
| $c$ | 6.721 | 6.758 | 6.591 | 6.613 | 6.711 |
| $V$ (Å$^3$) | 598.4 | 600.3 | 579.3 | 569.0 | 590.8 |

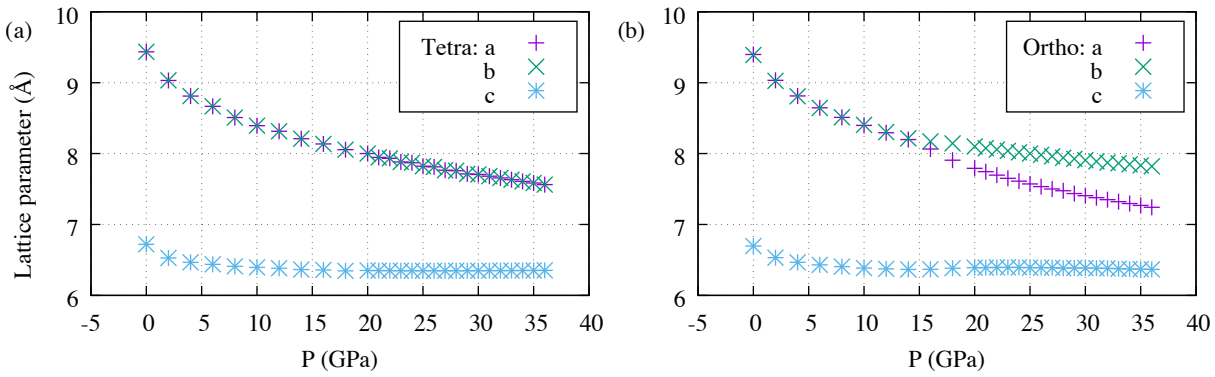


**FIGURE 1.** (a) Optimized lattice parameters of PETN based on a tetragonal initial structure using PBE+D3. (b) Same but with orthorhombic initial structures.

converged tetragonal structures at all pressures. The optimized lattice constants for hydrostatic pressures from 0 to 36 GPa are shown in Figure 1a. The lattice constants for PETN I at 0 GPa are compared with selected values from the literature in Table 1.

Optimizations initiated with the non-hydrostatic orthorhombic structure reported by Tschauner et al. [8] also resulted in tetragonal structures at pressures well above the expected onset of a stable orthorhombic phase. These optimizations reproduced the converged tetragonal structures demonstrating the uniqueness of the tetragonal structure. Only at significantly higher pressures (> 20 GPa) did these optimizations converged to an orthorhombic structure.

Subsequently, we used an orthorhombic structure relaxed at 30 GPa to re-initialize optimizations at all pressures. These resulting optimizations produced converged orthorhombic structures at progressively lower pressures, until they reverted to a tetragonal cell below 15 GPa. The fractional coordinates for the orthorhombic structure optimized at 20 GPa are given in Table 2. The optimized lattice constants for all pressures (thus including the tetragonal structures) are plotted in Figure 1b.

The tetragonal and orthorhombic structures converged at 20 GPa are compared in Figure 2. To facilitate the comparison, the structures were translated to superimpose the central carbon atoms of one of the PETN molecules in the unit cell. A symmetry analysis [28] confirmed that the tetragonal structure exhibits symmetry of the $P\bar{4}2_1c$ space group and the orthorhombic structure exhibits symmetry of the $P2_12_12$ space group, in agreement with prior deductions based on experimental data [4, 7, 8, 10].

Qualitatively, the differences between the tetragonal and orthorhombic phases can be decomposed into a relative translation of the two molecules in the unit cell and an internal change in molecular conformation. These two effects have been inferred separately in prior work, with XRD combined with group theory arguments supporting the static displacement of the whole PETN molecules [8] and with Raman spectroscopy combined with gas-phase DFT calculations supporting the internal conformational change [4, 10]. Our optimized structures indicate that, during the transition, translation of the molecular centers of mass occurs approximately along the $[\bar{1}10]$ direction with slight expansion along the $c$ axis. The internal change in conformation consists of inequivalent twisting of opposing pairs of nitro groups in each PETN molecule, resulting in the molecular symmetry reduction from $S_4$ to $C_2$, as confirmed by numerical analysis.

To assess the relative stability of the two phases, we calculated the enthalpies of the optimized structures, excluding ZPE, obtained at each pressure from the tetragonal and orthorhombic initial conditions: $H_{\text{tetra}}$ and $H_{\text{ortho}}$.

**TABLE 2.** Optimized fractional coordinates of the stable orthorhombic phase (PETN III) at 20 GPa using PBE-D3/DZVP. The optimized lattice parameters are $a$ = 7.792 Å, $b$ = 8.100 Å, and $c$ = 6.391 Å.

| Atom | Wyckoff label | $x$ | $y$ | $z$ |
|---|---|---|---|---|
| C1 | 2$a$ | 0.0000 | 0.0000 | 0.2486 |
| C2 | 4$c$ | 0.4242 | 0.6303 | 0.8877 |
| C3 | 4$c$ | 0.6385 | 0.5641 | 0.6106 |
| H1 | 4$c$ | 0.3019 | 0.5880 | –0.0483 |
| H2 | 4$c$ | 0.4051 | 0.7456 | 0.8040 |
| H3 | 4$c$ | 0.7606 | 0.5763 | 0.6911 |
| H4 | 4$c$ | 0.6026 | 0.6797 | 0.5340 |
| O1 | 4$c$ | 0.5397 | 0.6555 | 0.0621 |
| O2 | 4$c$ | 0.6548 | 0.4377 | 0.4518 |
| O3 | 4$c$ | 0.5874 | 0.8362 | 0.3097 |
| O4 | 4$c$ | 0.3873 | 0.8875 | 0.0758 |
| O5 | 4$c$ | 0.8253 | 0.3688 | 0.1975 |
| O6 | 4$c$ | 0.8744 | 0.5984 | 0.3741 |
| N1 | 4$c$ | 0.5005 | 0.8052 | 0.1560 |
| N2 | 4$c$ | 0.7966 | 0.4729 | 0.3309 |

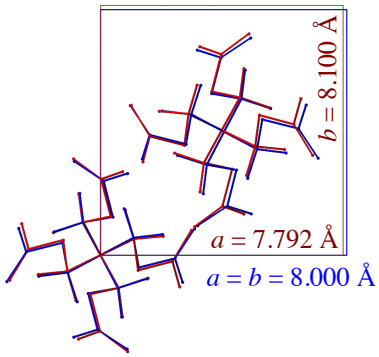


**FIGURE 2.** (a) The metastable tetragonal (blue) and stable orthorhombic (red) unit cells of PETN optimized at 20 GPa using PBE+D3, as viewed down the $c$-axis.

Calculations were performed using a variety of methods to re-optimize the structures, as described in the Computational Methods section, and resulting differences in the enthalpy values at each pressure are plotted in Fig. 3(a). In each series, both initial conditions yield the same optimized tetragonal structure at low pressures. However, above a certain pressure, the initial conditions lead to two different optimized structures of either tetragonal or orthorhombic symmetry. In all cases, the orthorhombic case is increasingly stable with pressure, and furthermore, the free energy changes continuously with respect to pressure through the phase transition. The difference in densities between the pairs of optimized structures is also plotted in Fig. 3(b) for three selected series of calculations, with analogous results. These results support both the experimental observations and the theoretical deductions based on symmetry arguments by Tschauner et al. [8], albeit at much higher pressures for the transition.

All of these calculations predict that the orthorhombic phase becomes more stable than the tetragonal phase at sufficiently high pressure. We find that the differences in methods do have a significant effect on the predicted relative stability of PETN I and III, with transition pressures ranging widely from about 16 to 23 GPa, based on linear fits to the enthalpy–pressure data. Calculations of higher accuracy within the PBE+D3 method (i.e., using the larger TZVP basis set, or using the larger $2 \times 2 \times 2$ supercell) predict higher transition pressures. On the other hand, calculations using the more sophisticated hybrid HSE functional lead to a lower transition pressure than any predicted using PBE. Both the D2 and D3 dispersion corrections also have the effect of lowering the predicted transition pressure compared

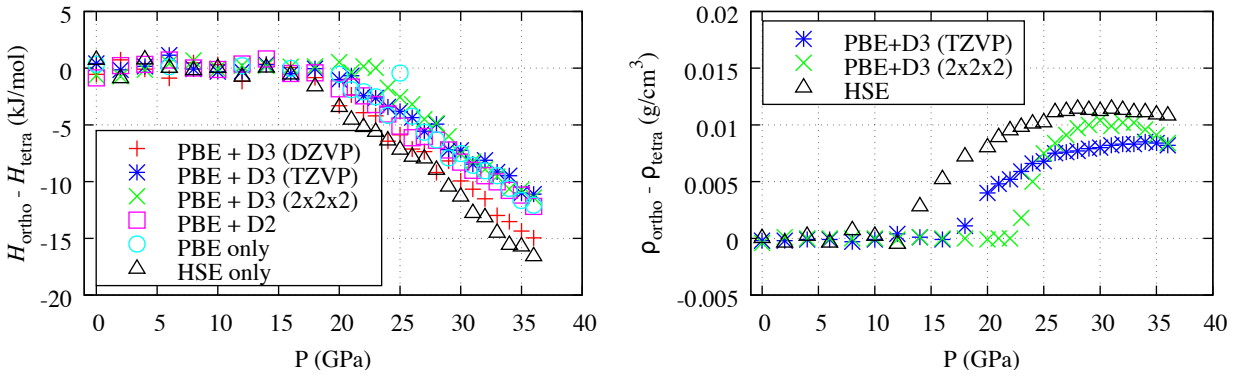


**FIGURE 3.** (a) The difference in enthalpies between optimized crystal structures obtained using initial conditions with tetragonal and orthorhombic symmetry. (b) The difference in densities between the same structures.

to calculations using PBE only.

Given the significant sensitivity of the results to the calculation details among reasonable choices of methods, we conclude that a quantitative prediction of the transition pressure is not yet possible based on the DFT calculations presented here. However, we observe that all methods produce qualitatively the same transition, with similar magnitudes in the differences in enthalpy. Furthermore, the entire range of predicted transition pressures is significantly higher than those observed experimentally for the PETN I→III transition near 5 GPa [4], 6 GPa [8], 7 GPa [7], and 9 GPa [10]. The transition may be observed to occur at yet higher pressures with further minimization of hydrostatic effects via the pressure medium, which experimental reports have identified as a likely cause for variations in the transition pressure [6, 10].

## CONCLUSIONS

We have presented DFT calculations of an orthorhombic phase of PETN found to be stable at pressures above 16 to 23 GPa. The predicted $P2_12_12$ symmetry of the converged orthorhombic structure matches the symmetry of the proposed PETN III phase based on Raman spectroscopy and XRD [4, 7–10]. Work is underway to incorporate zero-point energy and thermal corrections to refine the predicted stability of the orthorhombic phase as well as to calculate the XRD and Raman spectra to validate our predictions against the signatures of the PETN I to III phase transition observed in experiments. We are also investigating possible factors contributing to the variances in the predicted transition pressures with respect to the level of theory.

## ACKNOWLEDGMENTS

This work was supported by the Office of Naval Research (ONR), both directly (project N0001416WX00033) and through the U.S. Naval Research Laboratory (NRL). Computational resources were provided through NRL and the Department of Defense High Performance Computing Modernization Program. N.Q.L. is grateful for support from the National Research Council Research Associateship Programs.

## REFERENCES

[1] J. J. Dick, R. N. Mulford, W. J. Spencer, D. R. Pettit, E. Garcia, and D. C. Shaw, J. Appl. Phys. **70**, 3572–3587 (1991).
[2] J. J. Dick, J. Appl. Phys. **81**, 601–612 (1997).
[3] V. K. Jindal and D. D. Dlott, J. Appl. Phys. **83**, 5203–5211 (1998).
[4] Y. A. Gruzdkov, Z. A. Dreger, and Y. M. Gupta, J. Phys. Chem. A **108**, 6216–6221 (2004).
[5] J. Trotter, Acta Crystallogr. **16**, p. 698 (1963).

[6] K. E. Lipinska-Kalita, M. G. Pravica, and M. Nicol, J. Phys. Chem. B **109**, 19223–19227 (2005).
[7] M. Pravica, K. Lipinska-Kalita, Z. Quine, E. Romano, Y. Shen, M. F. Nicol, and W. J. Pravica, J. Phys. Chem. Solids **67**, 2159–2163 (2006).
[8] O. Tschauner, B. Kiefer, Y. Lee, M. Pravica, M. Nicol, and E. Kim, J. Chem. Phys. **127**, p. 094502 (2007).
[9] J. A. Ciezak and T. A. Jenkins, "New outlook on the high-pressure behavior of pentaerythritol tetranitrate," Tech. Rep. ARL-TR-4238 (U.S. Army Research Laboratory, 2007).
[10] Z. A. Dreger and Y. M. Gupta, J. Phys. Chem. A **117**, 5306–5313 (2013).
[11] E. A. Zhurova, A. I. Stash, V. G. Tsirelson, V. V. Zhurov, E. V. Bartashevich, V. A. Potemkin, and A. A. Pinkerton, J. Am. Chem. Soc. **128**, 14728–14734 (2006).
[12] R. V. Tsyshevsky, O. Sharia, and M. M. Kuklja, J. Phys. Chem. C **117**, 18144–18153 (2013).
[13] D. C. Sorescu, B. M. Rice, and D. L. Thompson, J. Phys. Chem. B **103**, 6783–6790 (1999).
[14] C. K. Gan, T. D. Sewell, and M. Challacombe, Phys. Rev. B **69**, p. 035116 (2004).
[15] W. F. Perger, J. Zhao, J. M. Winey, and Y. M. Gupta, Chem. Phys. Lett. **428**, 394–399 (2006).
[16] E. F. C. Byrd and B. M. Rice, J. Phys. Chem. C **111**, 2787–2796 (2007).
[17] M. W. Conroy, I. I. Oleynik, S. V. Zybin, and C. T. White, Phys. Rev. B **77**, p. 094107 (2008).
[18] D. C. Sorescu and B. M. Rice, J. Phys. Chem. C **114**, 6734–6748 (2010).
[19] J. M. Gonzalez, A. C. Landerville, and I. I. Oleynik, "Vibrational and thermophysical properties of PETN from first principles," in *AIP Conference Proceedings: Shock Compression of Condensed Matter*, Vol. 1793 (2017) p. 070009.
[20] J. A. Ciezak, E. F. Byrd, and B. M. Rice, "Exploring the high-pressure behavior of PETN: A combined quantum mechanical and experimental study," Tech. Rep. (U.S. Army Research Laboratory, 2006).
[21] J. VandeVondele, M. Krack, F. Mohamed, M. Parrinello, T. Chassaing, and J. Hutter, Comput. Phys. Commun. **167**, 103–128 (2005).
[22] J. P. Perdew, K. Burke, and M. Ernzerhof, Phys. Rev. Lett. **77**, 3865–3868 (1996).
[23] J. Heyd, G. E. Scuseria, and M. Ernzerhof, J. Chem. Phys. **118**, 8207–8215 (2003).
[24] S. Goedecker, M. Teter, and J. Hutter, Phys. Rev. B **54**, 1703–1710 (1996).
[25] C. Hartwigsen, S. Goedecker, and J. Hutter, Phys. Rev. B **58**, 3641–3662 (1998).
[26] S. Grimme, J. Comput. Chem. **27**, 1787–1799 (2006).
[27] S. Grimme, J. Antony, S. Ehrlich, and H. Krieg, J. Chem. Phys. **132**, p. 154104 (2010).
[28] H. T. Stokes and D. M. Hatch, J. Appl. Crystallogr. **38**, 237–238 (2005).
[29] B. Olinger, P. M. Halleck, and H. H. Cady, J. Chem. Phys. **62**, 4480–4483 (1975).